LANGMUIR

Article

Cite This: *Langmuir* 2019, 35, 2153−2163

pubs.acs.org/Langmuir

Enhancing Electrochemical Efficiency of Hydroxyl Radical Formation on Diamond Electrodes by Functionalization with Hydrophobic Monolayers

Austin H. Henke,[†] Timothy P. Saunders,[†] Joel A. Pedersen,[†,‡] and Robert J. Hamers*[,†]

[†]Department of Chemistry and [‡]Departments of Soil Science and Civil & Environmental Engineering, University of Wisconsin, Madison, Wisconsin 53706, United States

Supporting Information

ABSTRACT: Electrochemical formation of high-energy species such as hydroxyl radicals in aqueous media is inefficient because oxidation of H_2O to form O_2 is a more thermodynamically favorable reaction. Boron-doped diamond (BDD) is widely used as an electrode material for generating $^{\bullet}OH$ radicals because it has a very large kinetic overpotential for O_2 production, thus increasing electrochemical efficiency for $^{\bullet}OH$ production. Yet, the underlying mechanisms of O_2 and $^{\bullet}OH$ production at diamond electrodes are not well understood. We demonstrate that boron-doped diamond surfaces functionalized with hydrophobic, polyfluorinated molecular ligands (PF-BDD) have significantly higher electrochemical efficiency for $^{\bullet}OH$ production compared with hydrogen-terminated (H-BDD), oxidized (O-BDD), or poly(ethylene ether)-functionalized (E-BDD) boron-doped diamond samples. Our measurements show that $^{\bullet}OH$ production is nearly independent of surface functionalization and pH (pH = 7.4 vs 9.2), indicating that $^{\bullet}OH$ is produced by oxidation of H_2O in an outer-sphere electron-transfer process. In contrast, the total electrochemical current, which primarily produces O_2, differs strongly between samples with different surface functionalizations, indicating an inner-sphere electron-transfer process. X-ray photoelectron spectroscopy measurements show that although both H-BDD and PF-BDD electrodes are oxidized over time, PF-BDD showed longer stability (≈24 h of use) than H-BDD. This work demonstrates that increasing surface hydrophobicity using perfluorinated ligands selectively inhibits inner-sphere oxidation to O_2 and therefore provides a pathway to increased efficiency for formation of $^{\bullet}OH$ via an outer-sphere process. The use of hydrophobic electrodes may be a general approach to increasing selectivity toward outer-sphere electron-transfer processes in aqueous media.

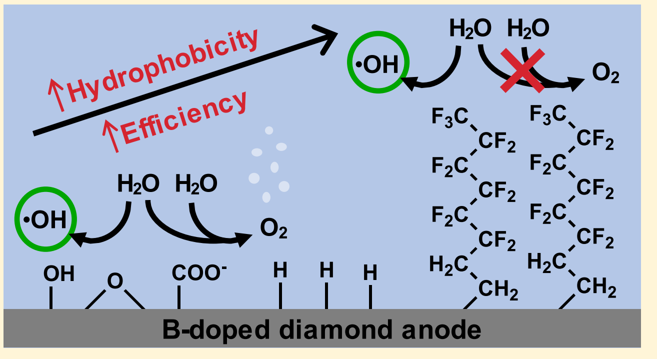

INTRODUCTION

The selective electrochemical formation of energetic chemical species is of great interest as one approach to induce chemical transformations in an energy-efficient manner.[1−6] The electrochemical formation of hydroxyl radicals ($^{\bullet}OH$) has emerged as a particularly important example because hydroxyl radicals are potent oxidants capable of oxidizing a wide variety of organic and inorganic contaminants at near-diffusion-limited rates,[7,8] leading to intense interest in the use of $^{\bullet}OH$ for applications such as water purification.[8−14] Electrochemical generation of $^{\bullet}OH$ possesses a number of advantages over existing water purification approaches in a large part because no reagents need to be added to produce the oxidant.

The Faradaic efficiency for $^{\bullet}OH$ production from H_2O is poor because the direct, one-electron reaction $H_2O \rightarrow {}^{\bullet}OH + H^+ + e^-$ has an associated standard reduction potential (E^0 = 2.74 V) that is unfavorable compared with the two-electron oxidation $H_2O \rightarrow H_2O_2 + 2H^+ + 2e^-$ (E^0 = 1.74 V) and the four-electron oxidation $H_2O \rightarrow O_2 + 4H^+ + 4e^-$ (E^0 = 1.23 V) processes. Since oxidation of water to form O_2 is the most thermodynamically favorable reaction, increases in production of $^{\bullet}OH$ must involve manipulation of the kinetic pathways, either by reducing the rate of the four-electron oxidation that produces O_2 or by increasing the rate of formation of $^{\bullet}OH$. Empirically, it is known that SnO_2,[15] PbO_2,[16,17] and boron-doped diamond (BDD)[13,14] are the electrode materials with highest efficiency for producing $^{\bullet}OH$. Of these, boron-doped diamond (BDD) is recognized as having the best overall performance because it produces aqueous $^{\bullet}OH$,[12−14,18] is chemically and physically robust,[19] and has a high kinetic overpotential for oxidation of water to O_2.[14,20−23]

Although it is known empirically that diamond is comparatively good at producing $^{\bullet}OH$ radicals, the detailed electrochemical pathways for forming $^{\bullet}OH$ and O_2 at diamond surfaces are not well understood,[13,14,21,24] inhibiting efforts to

Received: December 2, 2018
Published: December 14, 2018

DOI: 10.1021/acs.langmuir.8b04030
Langmuir 2019, 35, 2153−2163

identify materials that could be even more selective at producing •OH. A recent computational study examining water oxidation on metal oxides calculated the free energies of M−OH, M−O, and M−OOH intermediates (where M = metal) and reported that oxides with the largest free energy of formation of M−OH were most effective at forming hydroxyl radicals.[25] Yet, electrochemical reactions on diamond are quite distinct from those on metal oxides because although metal oxides have labile M−O and MO−H bonds that can transiently produce active surface sites to facilitate inner-sphere reactions, the C−H, C−O and CO−H bonds at diamond surfaces are very strong and nonlabile, disfavoring inner-sphere reaction pathways.[26,27] Density functional calculations have estimated the C−O and C−OH bond strengths at diamond surfaces to be 4−5 eV (400−500 kJ mol^{-1}), depending on the precise crystal face and surface coverage.[28] Similarly, the O−H dissociation constants K_a of aliphatic alcohols are small: $K_a \approx 10^{-18}$ for *tert*-butanol,[29] corresponding to free-energy changes of ∼100 kJ mol^{-1}. These values show that although oxidized BDD (O-BDD) surfaces may have a number of species,[30−34] these do not necessarily provide labile sites for inner-sphere electrochemical reactions.[26,27] One potentially important property controlling electrochemical pathways on diamond is surface hydrophobicity, which impacts the organization of the adjacent water molecules.[35,36] Surface hydrophobicity can be manipulated via direct fluorination of diamond[37−42] (F-BDD) and by functionalization with polyfluorinated ligands (PF-BDD).[43] These surface modifications have been shown to yield very hydrophobic surfaces with only very weak interaction with water.[35,36] The high C−F bond strength (calculated at 506 kJ mol^{-1})[44] suggests that using fluorinated surfaces or ligands provides a robust way to potentially alter the relative rates of O_2 and •OH production.

Here, we demonstrate that functionalization of conductive diamond surfaces with hydrophobic ligands significantly increases the efficiency of formation of •OH radicals. We formed hydrophobic electrodes by covalently linking polyfluorinated molecules to conductive, boron-doped diamond (BDD) surfaces and then compared the •OH production efficiencies of these functionalized surfaces with those of hydrogen-terminated (H-BDD), ether-terminated (E-BDD), and O-BDD surfaces. Figure 1 shows schematics of the four types of functionalized BDD analyzed. Electrochemical generation of •OH radicals was quantified using terephthalic acid (TPA), which selectively reacts with •OH to produce a single, easily detected product.[45−48] We demonstrate that functionalization of BDD anodes with hydrophobic, polyfluorinated ligands leads to a significant enhancement in electrochemical •OH production efficiency that persists even after 24 h of constant electrolysis. Our results suggest that a key to increasing efficiency for •OH production is to control the surface composition and structure in a manner that reduces the possibility of inner-sphere, multielectron oxidation steps that lead to O_2, without inhibiting the outer-sphere, single-electron oxidation pathway that produces •OH.

■ EXPERIMENTAL SECTION

Electrode Preparation. Experiments reported here used boron-doped, polycrystalline, electrochemical-grade diamond electrodes ($\rho < 2 \times 10^{-3}\ \Omega$ m, [B] $\approx 10^{20}$ atom cm^{-3}) purchased from Element Six. The freestanding BDD electrodes were cleaned by first soaking in aqueous piranha solution (3:1 v/v concentrated H_2SO_4/30% H_2O_2) overnight and then by rinsing with hydrofluoric acid (Sigma-Aldrich,

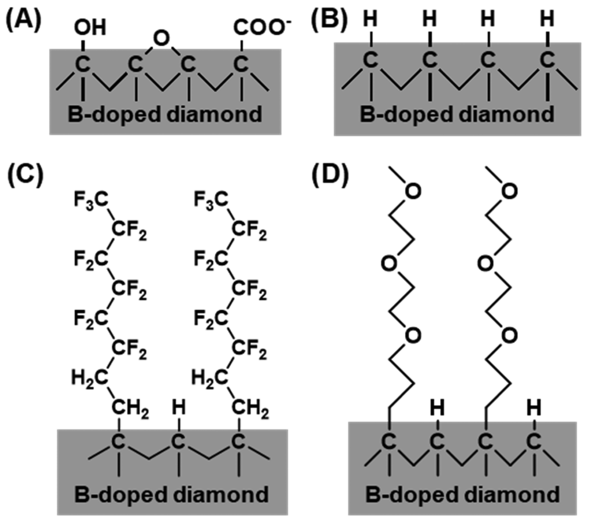

Figure 1. Schematic representations of surface functional groups for (A) oxygen-terminated, (B) hydrogen-terminated, (C) 1,1,2-*H*-perfluoro-oct-1-ene-terminated, and (D) allyloxy(diethylene oxide)-methyl-ether-terminated BDD.

48%), followed by nanopure water (Barnstead Genpure System, ρ > 18.2 MΩ cm). Samples were hydrogen-terminated by exposure to a pure hydrogen plasma in an Astex microwave chemical vapor deposition system using microwave power of 600 W ($T \approx 450$ °C) and pressure ∼3 Torr. The resulting H-terminated boron-doped diamond (H-BDD) samples were stored under dry argon between experiments to prevent surface oxidation or accumulation of H_2O in atmosphere. To produce oxygen-terminated BDD (O-BDD), H-BDD samples were placed in aqueous 30% H_2O_2 and illuminated with light from a low-pressure mercury ultraviolet (UV) lamp at 254 nm (UVP Pen-Ray Grid, 254 nm, ∼15 mW cm^{-2}) for at least 30 min.

We used photochemically initiated grafting of terminal organic alkenes[49−51] to functionalize H-BDD with polyfluorinated ligands and a poly(ethylene ether). H-BDD electrodes were placed in a stainless-steel reaction vessel under dry argon. The surface of the H-BDD sample was covered with a single reactant of interest, typically requiring 20−60 μL. The reactants used are 1,1,2-*H*-perfluoro-oct-1-ene ("PF-8", Alfa Aesar, 99%), 1,1,2-*H*-perfluoro-dec-1-ene ("PF-10", Alfa Aesar, 99%), and allyloxy(diethylene oxide)-methyl-ether (Gelest, 95%) that were previously dried using molecular sieves. The reaction vessel was sealed with a UV-grade fused silica window and illuminated with light from a UV lamp (similar to the above) for 24 h. The vessel was water-cooled to prevent evaporation of the reactant. Next, the electrode was removed from the vessel, soaked for 30 min each in chloroform (Sigma-Aldrich, 99.8%) and methanol (Fisher, 99.9%) to remove excess reactant, and dried under nitrogen to produce either a polyfluorinated BDD (PF-BDD) electrode or a poly(ethylene ether)-functionalized BDD (E-BDD) electrode. We performed control experiments with PF-BDD to quantify noncovalent adsorption to BDD using the same procedure as above, except without UV illumination.

We primarily report results for experiments with PF-8-functionalized BDD, which are referred to as PF-BDD. Most experiments were also conducted with PF-10-functionalized BDD, which yielded similar results to PF-8 BDD, indicating their behavior is characteristic of this class of molecules. See the Table S1 (Supporting Information (SI)) for a direct comparison. For selected experiments, E-BDD acts as a control, since it contains a monolayer of ligands similar in length to those of PF-BDD, but which are more hydrophilic. All experiments were performed in at least triplicates, and reported errors are a standard error of the mean from replicate samples.

Electrode Characterization. We determined the elemental composition of BDD surfaces using an ultrahigh vacuum X-ray photoelectron spectroscopy (XPS) system with a monochromatized

DOI: 10.1021/acs.langmuir.8b04030
Langmuir 2019, 35, 2153−2163

Al Kα X-ray source and a hemispherical analyzer. Survey spectra were obtained summing three scans with a binding energy step size of 1 eV and high-resolution spectra were obtained summing 20 scans with a step size of 0.125 eV. Casa XPS software was used for data analysis. For area quantification, peaks were fit to 70:30 Gaussian−Lorentzian functions with Shirley[52] background correction.

Electrode water droplet contact angles were measured using a Dataphysics OCA15 Goniometer with droplet volume of 8 μL and an application rate of 0.5 $\mu L\ s^{-1}$. SCA20 software was used to capture images and calculate angles for advancing, needle-in sessile droplets.

Electrochemical Measurements and Solutions. Electrochemical experiments were performed on a Metrohm Autolab 302N potentiostat−galvanostat, and data were analyzed using NOVA 1.6 software. To quantify the production of $^{\bullet}$OH, we used the oxidation of terephthalic acid (TPA) to 2-hydroxy-terephthalic acid (HTPA), for which the reaction is shown in the SI (Scheme S1). We used TPA specifically because (1) TPA does not directly oxidize on electrode surfaces as easily as other common $^{\bullet}$OH probes[53] and (2) a single product (HTPA) can be quantified via fluorescence. We prepared NaH_2PO_4/Na_2HPO_4 buffered solutions at pH 7.4 and 9.2 by adding H_3PO_4 (Sigma-Aldrich, 85% in H_2O) as needed to a solution of 0.1 M Na_2HPO_4 (Fisher, 99.8%) in nanopure water. These solutions were used to prepare 0.50 mM TPA stock solutions using disodium terephthalate (Alfa Aesar, 99%). Under our experimental conditions (pH 7.4), the reaction rate of $^{\bullet}$OH with TPA is over 100× faster than that for any suspected competing reaction, as determined from literature second-order rate constants[5] and approximate concentrations (SI, Table S2). The TPA solution was placed in the anode compartment and the buffer in the cathode compartment of an open-air, two-compartment cell with a finely porous glass frit separator. BDD was used as the working electrode, platinum mesh as the counter electrode, and 3 M Ag|AgCl as the reference electrode. Without stirring, a potential of 2.7 V versus standard hydrogen electrode (SHE) was applied to the working electrode for 30 min while measuring current (Δt = 0.5 s). Then, the electrolyte within the anode compartment was removed and analyzed via fluorescence. We explored the behavior over a range of potentials, and data shown here were obtained at 2.7 V. This potential was selected because it is close to the minimum needed to produce $^{\bullet}$OH at circumneutral pH (E^0 = 2.74 V; E = 2.3 V at pH = 7) and yielded higher efficiencies than more oxidizing potentials.

To further characterize differences in electrochemical performance, cyclic voltammetry (CV) was performed using functionalized BDD working electrodes in the same buffered TPA solution as above before and after a 30 min electrolysis in a one-compartment cell. For a given electrode, five scans were recorded at 50 $mV\ s^{-1}$ from +0.5 V → +3.5 V → −2.0 V → +0.5 V versus SHE. Then, 2.7 V versus SHE was applied for 30 min. Finally, the five scans were repeated as above, without changing the solution. A platinum disk was used as the counter electrode, and 3 M Ag|AgCl as the reference electrode.

Fluorescence Measurements. We measured fluorescence of HTPA using an ISS K2 spectrofluorimeter. Measurement conditions are similar to those used previously,[45−48] and were reproduced and optimized for our system. Emission spectra for HTPA solutions were measured from 340−550 nm using an excitation wavelength of 315 nm. The fluorescence spectrum exhibits a maximum at 422 nm. Quantification of HTPA was conducted by converting the fluorescence intensity at this wavelength to HTPA concentration using a calibration curve (Figure S1A, SI). Further information on fluorescence calibration and normalization procedures can be found in the SI. The UV−visible absorption spectra of TPA and HTPA reported both in our SI (Figure S1B) and in the literature[46] reveal that TPA displays negligible absorption at the excitation wavelength.

■ RESULTS AND DISCUSSION

Functionalization of BDD. X-ray photoelectron spectroscopy characterization of the surface composition of H-BDD, O-BDD, and PF-BDD yielded the results shown in Figure 2.

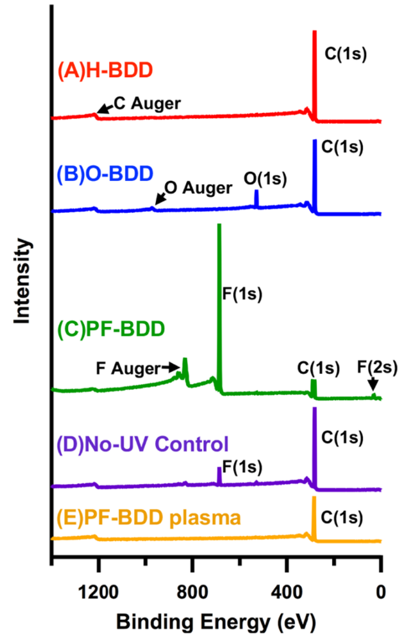

Figure 2. XPS spectra for (A) H-BDD, (B) O-BDD, (C) PF-BDD, (D) control sample exposed to PF without UV light, and (E) PF-BDD after cleaning with H_2 plasma.

Freshly prepared H-BDD (Figure 2A) shows a strong C(1s) peak near 282 eV and a C KVV Auger peak near 1220 eV, without any other detectable species except for a very small O(1s) feature near 529 eV. The spectrum for O-BDD (Figure 2B) is similar to that of H-BDD, with the addition of more intense O(1s) and O KLL Auger peaks around 529 and 974 eV, respectively, due to surface oxidation. After functionalizing H-BDD with polyfluoroalkene molecules, the spectrum (Figure 2C) exhibits strong F(1s) (686 eV) and F KLL Auger (832 eV) peaks. Furthermore, the high-resolution C(1s) spectrum for PF-BDD (Figure S2, SI) shows new peaks at higher binding energies than the diamond C(1s) peak corresponding to $C{-}F_2$ and $C{-}F_3$ species within the ligand layer. The F(1s) peaks and C(1s) subpeaks at higher binding energies for the PF-BDD samples and the absence of impurity peaks confirm that the diamond surfaces have been functionalized with the perfluorinated molecules. Upon functionalization of H-BDD with the poly(ethylene ether) ligands (E-BDD), the O(1s) peak near 529 eV increases in intensity compared to the starting H-BDD sample (Figure S3, SI) due to the presence of ether oxygen atoms. Unlike PF-BDD, E-BDD functionalization does not yield new peaks because the corresponding ligands contain only C and O.

We determined the density of PF molecules grafted to the BDD surface using the C(1s) and F(1s) peak areas of high-resolution XPS spectra and the equations described in the SI. These measurements yielded a molecular surface density for PF-BDD of 3.5 ± 0.3 molecule nm^{-2}. This is indistinguishable from the packing density of ∼3.5 molecules nm^{-2} observed for perfluorinated solid alkanes[54] but is significantly smaller than the ∼16 atom nm^{-2} density of carbon atoms on the diamond (111) surface. Our measured coverage is consistent with prior work from our group in which we established that the reaction conditions used here will covalently graft terminal alkenes to diamond surfaces, yielding monolayer films like those depicted in Figure 1C.[49,51,55−57] However, because the lattice spacing of diamond is less than the maximum packing density of

DOI: 10.1021/acs.langmuir.8b04030
Langmuir 2019, 35, 2153−2163

perfluorinated solid alkanes, the PF molecules cannot functionalize every C−H surface bond; as a consequence, some C−H surface sites are expected to remain unfunctionalized, as depicted in Figure 1C.[54] This nonideal packing and associated molecular disorder has important consequences for surface electron-transfer processes,[57] as will be discussed below.

As a control, Figure 2D shows an XPS spectrum of an H-BDD sample that was exposed to the PF ligand but not illuminated with UV light; this control sample shows a much lower F(1s) signal compared to that of PF-BDD with UV illumination (Figure 2E). This experiment further confirms that UV induces covalent grafting of PF molecules to the BDD surface, as depicted in Figure 2C.[51,55]

One attractive feature of BDD as a substrate is that samples can be reused many times, as the molecular ligands can be removed and the hydrogen termination restored by exposing the sample to hydrogen plasma. Figure 2E shows an XPS spectrum of a PF-BDD sample (like that in Figure 2C) that was then exposed to H_2 plasma (600 W total microwave power) for 1 h. Analysis of the F(1s) region shows that more than 99% of the surface F has been removed and the sample is chemically indistinguishable from a clean control sample. Scanning electron microscopy images (Figure S4, SI) further show that H_2 plasma treatment does not affect the morphology of polycrystalline BDD. In multiple studies, we established that BDD samples can be functionalized and H-plasma cleaned many times with no detectable change in electrochemical behavior.

Faradaic Efficiency of $^{\bullet}$OH Production on Functionalized BDD. We probed the production of $^{\bullet}$OH by BDD samples functionalized with each molecule by electrolyzing solutions containing TPA and then quantifying the HTPA produced. We also measured electrolytic current as a function of time ($I(t)$). Since the number of HTPA molecules observed is much less than the total number of electrons passed (mol $e^- = \frac{1}{F}\int I(t)\,dt$, where F is Faraday's constant), most of the current is associated with other oxidation reactions such as oxidation of water to O_2. Therefore, we use electrolytic current as an indirect measure of O_2 production. The Faradaic efficiency (η) for HTPA production during electrolysis is defined as

$$\eta = \frac{CVF}{\int I(t)\,dt} \tag{1}$$

where C is the measured final concentration of HTPA, V is the solution volume within the anode compartment, and F is Faraday's constant. In this context, η is the fraction of electrons that produces HTPA and $\eta \ll 1$ due to the dominance of oxygen evolution.

To estimate how η relates to $^{\bullet}$OH generation efficiency, we measured the rate of HTPA production as a function of [TPA] (Figure S5A, SI) for 30 min electrolyses and found that HTPA production increases linearly with [TPA] at low concentration (e.g., 0.5 mM) and plateaus become independent at high [TPA] (~5 mM). We assign this as a first-order reaction of $^{\bullet}$OH and TPA with respect to TPA that becomes pseudo zero order at high [TPA]. Since [$^{\bullet}$OH] ≪ [TPA], we assume that in the plateau region, all $^{\bullet}$OH is captured to produce HTPA. The TPA concentration used herein (0.5 mM) falls within the linear region of Figure S5 and yields an $^{\bullet}$OH capture efficiency of ~20%. Therefore, our reported Faradaic efficiencies for HTPA generation are a minimum for absolute $^{\bullet}$OH generation efficiency, which is likely 5× higher. Finally, we note that the above deviation in HTPA generation from linearity at high concentrations is not due to self-absorption or molecular aggregation of HTPA, as absorbance of HTPA is linear with [HTPA] for the full concentration range tested (Figure S5B, SI).

Figure 3 shows Faradaic efficiencies, whereas Figure 4 shows the corresponding HTPA production and the total electro-

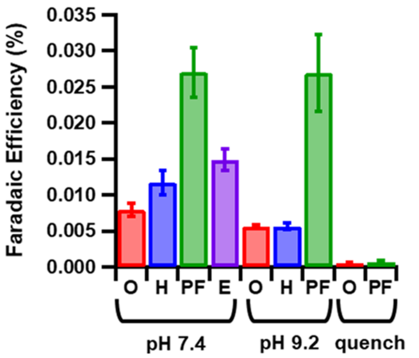

Figure 3. Faradaic efficiencies for formation of HTPA from functionalized diamond surfaces averaged over 30 min electrolyses at an applied potential of 2.7 V vs SHE. E-BDD was only tested at pH = 7.4. Quenched experiments were performed for O-BDD and PF-BDD at pH 7.4 by adding 0.3 M to the electrolyte.

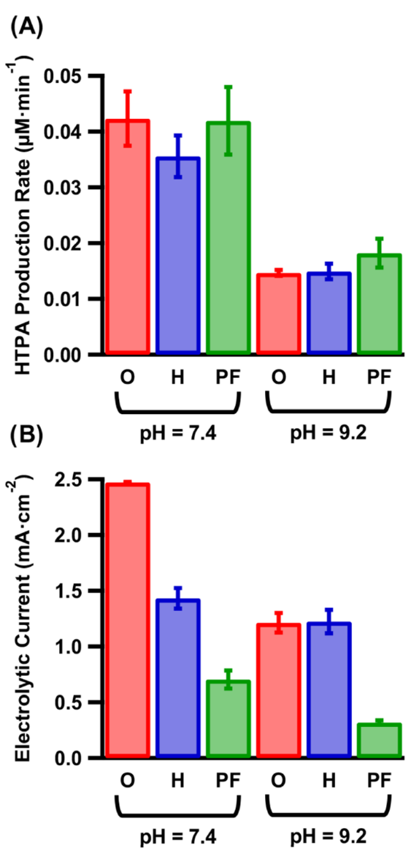

Figure 4. (A) HTPA production rates and (B) electrolytic currents for functionalized diamond surfaces averaged over 30 min electrolyses at an applied potential of 2.7 V vs SHE.

DOI: 10.1021/acs.langmuir.8b04030
Langmuir 2019, 35, 2153−2163

chemical charge passed (all values totaled over 30 min) for the different BDD samples at pH = 7.2 and 9.2. We first consider the influence of surface functionalization. At pH = 7.4, Figure 3 shows that PF-BDD electrodes produce •OH with significantly higher Faradaic efficiency than that of O-BDD, H-BDD, or E-BDD electrodes. Figure 4A shows that the rate of HTPA production does not differ significantly ($p > 0.05$) among BDD electrodes. Yet, the electrolytic current (Figure 4B) varies markedly, with PF-BDD yielding much lower current than H-BDD or O-BDD at both pH values tested. The trend in average electrolytic current is consonant with that observed for measured efficiencies in Figure 3. PF-BDD has the lowest electrolytic current and the highest Faradaic efficiency, whereas O-BDD has the highest electrolytic current and the lowest Faradaic efficiency. Similar trends are observed when comparing the differently functionalized surfaces at pH = 9.2.

Since production of HTPA (a proxy for •OH) is nearly independent of surface functionalization, we conclude that •OH production likely occurs by an outer-sphere electron-transfer process. In contrast, the strong dependence of the total electrolytic current (which primarily reflects production of O_2) on surface functionalization indicates that O_2 production occurs by an inner-sphere process. We conclude that PF-BDD has the highest Faradaic efficiency among the tested surfaces because the PF layer is most effective at inhibiting oxygen evolution.

Figure 3 also shows the results of quenching experiments performed with O-BDD and PF-BDD. In these experiments, electrolyses were conducted just as described, except with *t*-butanol (*t*-BuOH, 0.3 M) added to the electrolyte. *t*-BuOH is an effective •OH scavenger also resistant to direct oxidation on the electrode surface,[58] so this experiment was conducted to further ensure that •OH oxidation produces HTPA. Our results show that the addition of *t*-BuOH dramatically decreases HTPA generation efficiency for both O-BDD and PF-BDD, suggesting that HTPA is generated from reaction of TPA with •OH and that the presence of *t*-BuOH prevents this reaction. A comparison of the electrolytic currents and HTPA production rates for the quenching experiments with other experiments is in Figure S6, SI.

Effect of pH on Water Oxidation for Functionalized BDD. We now consider the influence of pH. In Figure 4, the data show that increasing the concentration of hydroxyl anions 60-fold (increasing from pH = 7.4 to 9.2) leads to modest decreases in both HTPA production and in electrolytic current, and Figure 3 shows a concurrent decrease in the Faradaic efficiency for HTPA production. The pH 7.4 and 9.2 solutions have nearly the same ionic strength ($I_{\mathrm{pH}\ 7.4} \approx 28$ mM, $I_{\mathrm{pH}\ 9.2} \approx 25$ mM) such that differences in solution conductivity are negligible. The observed influence of increasing pH is contrary to what would be expected if •OH was formed primarily from oxidation of OH^-. Therefore, we conclude that the •OH radicals that we detect arise from oxidation of H_2O and not from oxidation of hydroxyl anions.

The above interpretation assumes that the fluorescence quantum yield of HTPA does not depend strongly on pH within the range tested. Figure S7 (SI) shows that the fluorescence intensities of standard HTPA solutions are nearly constant for $6 < \mathrm{pH} < 12$, in agreement with prior work.[48] Therefore, we conclude that differences in fluorescence between solutions of pH = 7.4 and 9.2 are due to differences in HTPA concentration, further confirming our conclusion that the •OH we detect is produced by oxidation of H_2O and not by oxidation of OH^-.

Cyclic Voltammetry of Functionalized BDD Electrodes. Cyclic voltammetry (CV) was performed with each type of functionalized BDD before and after electrolysis to observe the solvent potential window, background current, and any possible changes to these with use. Figure 5A–D shows the first scan of the CVs before electrolysis. The applied potential for all electrolyses is shown as a dotted line in these graphs for comparison. PF-BDD's solvent window remains wider in subsequent scans (data not shown). The peaks around +2 V in the forward sweep for O-BDD, H-BDD, and E-BDD are attributed to oxidation of carbon atoms on the diamond surface. No other major peaks were observed, indicating an absence of interfering electrochemical processes. In all subsequent scans (data not shown), these surface oxidation peaks remain present. We hypothesize that in the negative sweep of the same scan (e.g., −2 V), the electrode surface becomes reduced such that in the positive sweep of the following scan, a similar surface oxidation peak emerges. CVs with O-BDD and H-BDD electrodes after 30 min electrolyses (Figure 5E,F), when the surface is likely fully oxidized, further support this conclusion. The first scan after electrolysis does not contain the surface oxidation peak, whereas the second scan (after running the reductive sweep of scan 1) does show the same surface oxidation peak. This eliminates the possibility that the peak instead corresponds to direct oxidation of TPA on the electrode surface. Notably, PF-BDD does not contain the electrode surface oxidation peak for any scans and maintains a widened solvent window over multiple scans. This indicates that PF functionalization is relatively stable against oxidation, as will be discussed below.

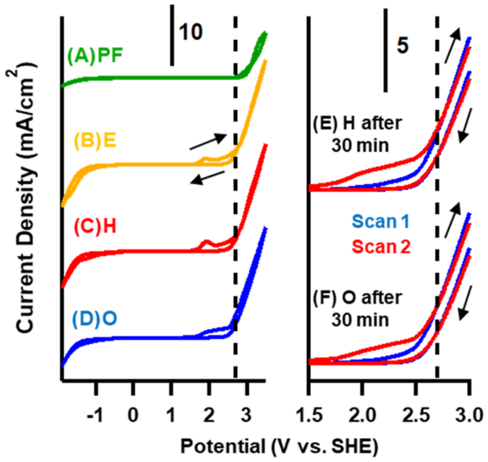

Figure 5. (A–D) First CV at 50 mV s^{-1} for PF-, E-, H-, and O-BDD before electrolysis. (E, F) The first and second scans for H- and O-BDD after a 30 min electrolysis. In both graphs, the dotted line corresponds to the potential at which all electrolyses are run (2.7 V). The arrows indicate the sweep direction, which is consistent in (B)–(D).

The background current regions (0 to +1 V) for several CVs are shown in Figure S8, SI. PF-BDD exhibits an order of magnitude (over 10×) lower background current than that of H-BDD and O-BDD, which are themselves similar. This is an interesting result because low background currents are desirable for electrochemical sensing, and although BDD is known to yield low background current,[22] PF functionalization

DOI: 10.1021/acs.langmuir.8b04030
Langmuir 2019, 35, 2153–2163

decreases it further. Background currents for each electrode type change minimally after 30 min electrolyses, indicating that electrode fouling with organic byproducts plays little role in changing performance (discussed below).

Changes in BDD Surface Functionalization during Electrolysis. To understand how the chemical nature of BDD surfaces change during electrolysis, we used XPS and quantified the areas for the C(1s), F(1s), and O(1s) peaks. Figure S9 (SI) shows representative spectra used in this analysis. Using these areas and the associated sensitivity factors, we determined the fraction of each element before and after 30 min electrolysis at 2.7 V versus SHE (also after 24 h for PF-BDD only), yielding the data in Figure 6.

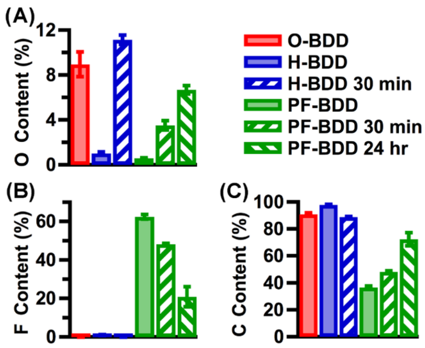

Figure 6. Surface content of (A) oxygen, (B) fluorine, and (C) carbon for functionalized BDD surfaces. For H- and PF-terminated samples, the data are shown before (start) and after electrolysis for 30 min. For PF-BDD, a sample is shown after 24 h of continuous electrolysis. All samples are held at 2.7 V vs SHE.

Freshly prepared H-BDD and PF-BDD contain minimal (<1%) surface oxygen content, whereas O-BDD contains 9.0 (±1.1)% oxygen (Figure 6A). Electrolysis of H-BDD transforms its surface to become similar to, yet distinguishable from, that of O-BDD. After only a 30 min electrolysis, H-BDD becomes oxidized, showing higher surface oxygen content than that of O-BDD (Figure 6A); that is, the electrochemical oxidation route produces a larger fraction of surface oxygen than the chemical oxidation route (H_2O_2/UV). Some insights into the nature of the oxidized sites can be gleaned from the presence of a Na(1s) peak near 1068 eV in the XPS spectrum of H-BDD after electrolysis (Figure S10, SI). Goeting et al.[34] observed a similar peak on oxidized BDD via XPS and attributed it to Na^+ bonded to deprotonated carboxylate groups. Since Na^+ is a component of our electrolyte and we detect it via XPS without detecting a significant P(2p) peak (thereby ruling out the presence of sodium phosphate species), we believe the Na we observe is associated with carboxylate groups formed during electrolysis. Notably, the XPS spectrum of an O-BDD sample that has been placed in the same Na^+-containing buffer for the same length of time as the electrolyte (Figure S10, SI) exhibits a negligible Na(1s) peak. Prior studies have shown that electrochemical oxidation of H-BDD yields a mixture of different oxygen-containing functional groups, including alcohols, ethers, and carboxylic acids.[30−34] Under the conditions of our experiments, electrochemical oxidation of H-BDD produces more total oxygen and more carboxylate groups than those in H_2O_2/UV treatment.

The F(1s) data in Figure 6B show loss of F content on the PF-BDD samples upon electrolysis, consistent with a prior electrochemical study of BDD terminated directly with F atoms.[59] In addition, Figure 6A shows that the O(1s) content of PF-BDD increases with electrolysis time. These changes indicate partial removal of surface-attached PF molecules or molecular fragments from BDD and subsequent oxidation of surface C−H_X groups to form oxygen-containing functional groups during electrolysis. In our system, loss of F can in principle arise from either (1) individual fluorine atom abstraction by $^\bullet$OH or (2) removal of ligands by cleavage of C−C bonds. Prior work on the oxidation of fluorinated surfactants by $^\bullet$OH and other species reported that completely perfluorinated chains were inert to such chemical oxidation, whereas molecules that were only partially fluorinated were degraded into shorter fluorinated alcohols via C−C bond cleavage.[60] The molecules we use in our studies are completely fluorinated except for the terminal alkene group bonded to the surface. Thus, we believe that loss of F most likely arises from $^\bullet$OH radicals attacking the $-H_2C-CH_2-$ group immediately adjacent to the diamond surface and removing ligands from the surface. Once perfluorinated ligands are removed during electrolysis, exposed $C_{diamond}$−H groups at the diamond surface (see Figure 1C) can be oxidized via H atom abstraction, followed by reaction with water.[61] Even though electrolysis induces loss of F and surface oxidation, the oxygen content of a PF-BDD surface after 30 min is much lower than that for H-BDD. Even after 24 h of electrolysis, the surface oxygen content of PF-BDD is less than that of H-BDD used for only 30 min. From this, we conclude that PF-BDD is significantly more resistant to oxidation than H-BDD under our experimental conditions, due to the protective monolayer. Overall, these XPS results are fully consistent with our CV results above, since H-BDD and O-BDD exhibit surface oxidation peaks and PF-BDD does not.

Contact angles represent one way to characterize changes in diamond surface functionalization and associated properties such as hydrophobic character.[33,38,62−64] Figure 7 shows contact angle data for functionalized samples before and after a 30 min electrolyses at 2.7 V versus SHE (representative images for these data can be found in the Figure S11, SI). The contact angle for O-BDD after electrolysis (data not shown) is very similar to that for O-BDD before electrolysis. As expected, the initial contact angles are in the order O-BDD < H-BDD < PF-BDD. After electrolysis, the contact angles for PF-BDD and for H-BDD both decrease. However, the value for PF-BDD still remains higher than that for the other surfaces; this is consistent with the XPS data indicating that PF-BDD is more resistant to oxidation compared with H-BDD.

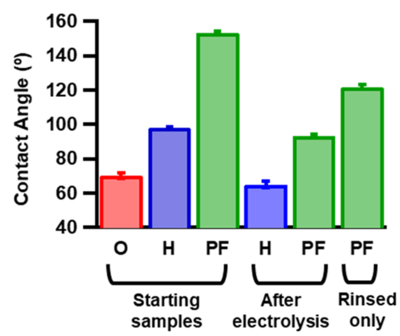

Figure 7. Contact angles for functionalized diamond surfaces interacting with water before and after a 30 min electrolyses and for PF-BDD samples rinsed with electrolyte (no electrolysis).

DOI: 10.1021/acs.langmuir.8b04030
Langmuir 2019, 35, 2153−2163

We also found that PF-BDD samples that were immersed in electrolyte without undergoing any electrolysis also underwent a small decrease in the contact angle compared to that in the initial surface. Time-dependent chronoamperometry experiments (Figure S12, SI) reveal that PF-BDD exhibits an increase in electrolytic current over the first several minutes. The contact angle and chronoamperometry results together suggest that within several minutes after immersion, water molecules partially intercalate into the perfluorinated film of the PF-BDD surface. This intercalation, in addition to oxidation, may contribute to the increase in O(1s) emission observed in XPS after electrolysis of the PF-BDD sample (Figure 5A).[59]

Changes in •OH and O_2 Formation with Electrode Use. To determine how changes in the surface of BDD electrodes affect electrochemical performance, we examined HTPA production from PF-BDD and H-BDD samples during three sequential 30 min electrolyses and from a 30 min electrolysis at the end of an extended (24 h) electrolysis for PF-BDD as a long-term ("LT") control. In each case, TPA was added to the cell at the beginning of the 30 min period under investigation. Example current versus time plots are in the SI (Figure S12). From these measurements, we extracted the HTPA production rate, the total electrolytic current, and the Faradaic efficiency for HTPA production (Figure 8A−C, respectively).

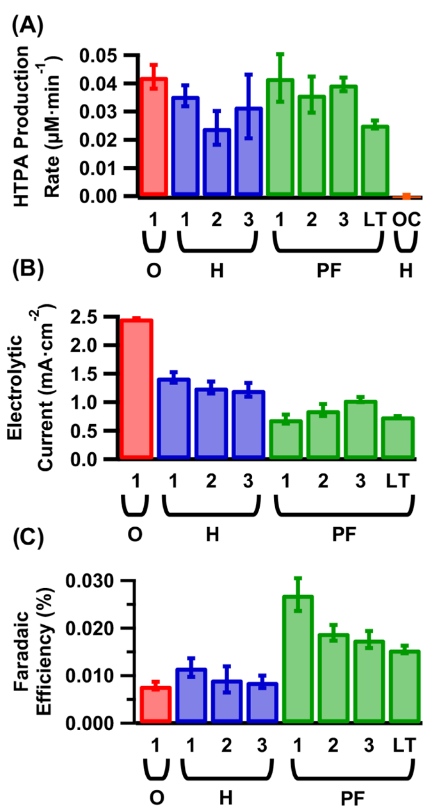

Figure 8. (A) HTPA production rates, (B) electrolytic currents, and (C) Faradaic efficiencies for each of three sequential 30 min electrolyses ("1−3", respectively) at applied potential of 2.7 V vs SHE and pH 7.4 for functionalized BDD electrodes. The open-circuit 30 min control (OC) involves no applied potential. The long-term ("LT") samples refer to 30 min electrolyses that were conducted on PF-BDD electrodes after 24 h of continuous electrolysis at 2.7 V.

Figure 8A shows that the HTPA production rate does not change significantly with electrode use. The HTPA production rate did not differ significantly ($p > 0.05$) between the multiple time points for H-BDD or PF-BDD except after 24 h for PF-BDD. This is surprising, given that Figures 6 and 7 show that the surface termination changes significantly with use over this period. These results suggest that the rate of •OH production, as measured by the increase in HPTA concentration, does not depend strongly on surface termination. To confirm that the HTPA we detected arose from electrochemical processes, we conducted an open-circuit control in the same manner as all electrolyses, except without an applied potential. The resulting HTPA detected in this control experiment (Figure 8A, "OC") is indistinguishable from the background, confirming that HTPA in other experiments is generated electrochemically.

Although Figure 8A shows that the HTPA production rate does not change significantly with time, Figure 8B shows that the electrolytic current for PF-BDD increases over multiple electrolyses, approaching the relatively constant electrolytic current of H-BDD. Consequently, as the electrolytic current of PF-BDD increases with use, the efficiency of HTPA production (Figure 8C) decreases and approaches that of H-BDD. These results further indicate that functionalization of diamond with hydrophobic ligands enhances the efficiency of •OH production by inhibiting O_2 formation and not by directly increasing •OH production rate. Moreover, even though the PF ligands may degrade, the efficiency for •OH production on PF-BDD remains higher than that of either H-BDD or O-BDD for multiple 30 min electrolyses. We also note that the electrolytic current for H-BDD after multiple electrolyses is still much lower than that of O-BDD, despite showing similar surface oxygen fractions (Figure 6A) and contact angles (Figure 7A). These results suggest that although H-BDD may become oxidized with use, the precise identity of the oxygen functional groups on the surface impacts the O_2 formation rate and these functional groups depend on the sample history.

Mechanistic Insights into Reactions on BDD Surfaces. Our results show that the total electrolytic current is strongly dependent on the surface functionalization and increases in the order PF-BDD < E-BDD < H-BDD < O-BDD. In contrast, formation of •OH remains relatively constant across the different surface functionalizations. On the basis of these observations, we conclude that the primary manner in which PF functionalization increases the efficiency of •OH production is by reducing the rate of the competing reaction, production of O_2.

Although the precise nature of the surface sites needed to form •OH and O_2 are unknown, we draw on recent computational studies investigating water oxidation on metal oxides.[25] On the basis of that work, we conjecture that the four elementary steps in O_2 formation on diamond may be

$$\mathrm{C{-}OH} \rightarrow \mathrm{C{-}O} + \mathrm{H^+} + \mathrm{e^-} \tag{2}$$

$$\mathrm{C{-}O} + \mathrm{H_2O} \rightarrow \mathrm{C} - \mathrm{OOH(hydroperoxy)} + \mathrm{H^+} + \mathrm{e^-} \tag{3}$$

$$\mathrm{C{-}OOH} \rightarrow \mathrm{C^{\bullet}(surface\ radical)} + \mathrm{O_2} + \mathrm{H^+} + \mathrm{e^-} \tag{4}$$

$$\mathrm{C^{\bullet}} + \mathrm{H_2O} \rightarrow \mathrm{C{-}OH} + \mathrm{H^+} + \mathrm{e^-} \tag{5}$$

In this model, an oxidized surface site, such as a surface C−OH group, acts as an inner-sphere site for O_2 production. We note

DOI: 10.1021/acs.langmuir.8b04030
Langmuir 2019, 35, 2153−2163

that eq 2 is not a simple alcohol deprotonation but is an electrochemically driven deprotonation to form a species akin to an adsorbed OH radical. On H-BDD, a well-terminated surface initially has few C−OH sites and therefore almost no sites for O_2 formation. However, such sites can be formed in situ, as $^{\bullet}$OH radicals that are formed (by an outer-sphere process) can abstract H atoms from surface C−H groups, leaving behind C "dangling bonds" that can then react with water, leading to gradual oxidation of the surface.[61] This initiation process can be described by eqs 6 and 7 below

$$\mathrm{C{-}H} + {}^{\bullet}\mathrm{OH} \rightarrow \mathrm{C}^{\bullet}(\text{surface radical}) + \mathrm{H_2O} \quad (6)$$

$$\mathrm{C}^{\bullet} + \mathrm{H_2O} \rightarrow \mathrm{C - OH} + \mathrm{H^+} + \mathrm{e^-} \quad (7)$$

By a similar argument, we propose that PF-BDD yields even lower electrolytic current (i.e., less O_2) by performing two essential functions: (1) the hydrophobic PF ligands block water molecules from approaching the diamond surface by providing less favorable intermolecular interactions and steric hindrance, and (2) the PF ligands act as a diffusion barrier that reduces the ability of $^{\bullet}$OH radicals to reach the diamond surface. Both properties must contribute, as our experiments with E-BDD (a more hydrophilic monolayer that still acts as a diffusion barrier) yielded a Faradaic efficiency for HTPA production moderately improved compared to that of O-BDD but significantly less than that for PF-BDD (Figure 3). The same properties (hydrophobicity and diffusion barrier) likely give PF-BDD the widest solvent potential window (Figure 5) and lowest background current (Figure S8, SI) of all tested electrodes. These electrochemical characteristics make functionalization of BDD with hydrophobic ligands not only promising for enhanced $^{\bullet}$OH generation efficiency but also for electrochemical sensing applications. The particular PF ligand we used has C−H species at the terminal alkene group (near the diamond interface) that may be a site for attack by $^{\bullet}$OH, leading to eventual degradation and loss of the PF layer.

Our arguments that hydrophobic molecular layers inhibit inner-sphere reactions are supported by two prior studies. Gayen et al.[43] showed that hydrophobic, perfluorinated monolayer on BDD blocked ClO_3^- from reaching the electrode surface, while still allowing for $^{\bullet}$OH formation.[43] Zhao et al. also reported that modification of PbO_2 anodes with hydrophobic fluorine resin increased oxygen evolution overpotential and thereby increased $^{\bullet}$OH production efficiency.[17] Taken together, they suggest that the use of hydrophobic layers to inhibit inner-sphere reactions in aqueous media may be a general phenomenon.

The independence of $^{\bullet}$OH generation to BDD surface functionalization is similar to the behavior observed for other redox couples that undergo characteristic outer-sphere electron-transfer reactions (e.g., $Ru(NH_3)_6^{3+/2+}$).[22,65,66] In our case, an outer-sphere reaction indicates that $^{\bullet}$OH forms from oxidation in solution near the electrode surface, without any direct bond formation to the surface. In addition, we found $^{\bullet}$OH production to decrease at higher pH, indicating that $^{\bullet}$OH is formed from H_2O and not OH^-. Therefore, we propose that $^{\bullet}$OH radicals are formed via an outer-sphere oxidation of H_2O to the H_2O^+ intermediate, which then decomposes to $^{\bullet}$OH and H^+

$$\mathrm{H_2O} \rightarrow \mathrm{H_2O^+} + \mathrm{e^-} \quad (8)$$

$$\mathrm{H_2O^+} \rightarrow {}^{\bullet}\mathrm{OH} + \mathrm{H^+} \quad (9)$$

Previous studies of plasmas formed in water have demonstrated the presence of H_2O^+.[67] Previous studies on radiolytic[68,69] and electrolytic[70] water oxidation phase have proposed H_2O^+ as an intermediate that decays through eq 9.[70] The outer-sphere pathway given by eq 8 must allow H_2O to approach sufficiently close to the BDD surface to initiate an electron-transfer process. Our contact angle, chronoamperometry, and XPS results all suggest that some water is able to penetrate into the molecular layer. These observations are consistent with previous molecular dynamics studies of molecular ligands on diamond surfaces,[57] showing that because the packing density of molecules is not well lattice-matched to the density of surface C atoms, the molecular layers formed on diamond have increased structural disorder compared with, e.g., self-assembled monolayers on gold. The increased disorder on diamond leads to layers in which the molecules have a high degree of conformational flexibility, opening gaps that allow water to penetrate closer to the surface than would be inferred from the static length of a stretched-out, static surface ligand. Water molecules that partially penetrate into the molecular layer can be oxidized in an outer-sphere process to produce $^{\bullet}$OH radicals, which can then either diffuse back into solution or penetrate all the way to the diamond surface to induce oxidation of residual C−H sites. The resulting oxidized sites likely play a role in the inner-sphere oxidation of water to O_2.

■ CONCLUSIONS

The primary conclusions drawn from this study can be summarized as follows. First, oxygen evolution and $^{\bullet}$OH production under our experimental conditions both arise from oxidation of H_2O and not OH^-. Second, $^{\bullet}$OH production on BDD does not depend strongly on surface termination, indicating that $^{\bullet}$OH production occurs via an outer-sphere electron-transfer process. Third, oxygen evolution on BDD varies strongly with surface functionalization. Finally, hydrophobic surface ligands protect the underlying, unreacted C−H sites from attack by hydroxyl radicals and/or other chemically reactive species.

A key aspect of our work is that formation of $^{\bullet}$OH can be accomplished by one-electron oxidation of H_2O, as illustrated in eqs 8 and 9. In contrast, formation of O_2 involves a more complex, four-electron process that necessarily has a more complex pathway involving multiple, sequential electron-transfer steps, like those indicated in eqs 2−5.[25] As a result, formation of O_2 is disfavored by the absence of surface functional groups (such as C−OH) that can form the necessary intermediates.[25] Functionalization of the surface with strongly hydrophobic ligands reduces the number of surface sites that are able to participate in inner-sphere reactions, while also creating a barrier region in which unfavorable intermolecular interactions block H_2O molecules from reaching surface active sites. The ligands may also have a protective effect, reducing the ability of $^{\bullet}$OH radicals to directly attack the diamond surface, which could then create labile sites for inner-sphere processes.

This work suggests that the use of hydrophobic ligands may provide a general pathway toward increasing the efficiency of outer-sphere electron-transfer processes. Selective production of $^{\bullet}$OH is of great interest because of the ability of this radical to mineralize organic contaminants and sterilize water, in processes generally referred to as electrochemical advanced oxidation processes.[7,9−14,71] However, the ability to alter

DOI: 10.1021/acs.langmuir.8b04030
Langmuir 2019, 35, 2153−2163

electrochemical kinetics to favor outer-sphere reactions has wider application in electrochemical synthesis and detection, as the ability to decrease formation of O_2 should facilitate enhanced efficiency for other electrochemical oxidation processes of soluble species that lie well beyond the 1.23 V stability limit of water.

■ ASSOCIATED CONTENT

Supporting Information

The Supporting Information is available free of charge on the ACS Publications website at DOI: 10.1021/acs.langmuir.8b04030.

(1) Table comparing experimental results between PF-8- and PF-10-functionalized BDD, (2) reaction scheme for the hydroxylation of terephthalic acid, (3) table of rate constants and reaction rates of relevant species with •OH, (4) fluorescence calibration curve, (5) TPA/HTPA UV−visible absorption spectra, (6) high-resolution C(1s) XPS spectrum of PF-BDD, (7) O(1s) comparison of XPS spectra for E-BDD and H-BDD, (8) scanning electron microscopy images of BDD electrodes, (9) plots of HTPA production rate as a function of TPA concentration and absorbance of HTPA as a function of concentration, (10) HTPA production rates and average electrolytic currents for *t*-BuOH-quenched electrolyses compared to those in nonquenched electrolyses, (11) plot of fluorescence intensity vs pH for standard HTPA solutions, (12) the background current regions of first-scan CVs before and after electrolysis (13) representative high-resolution XPS spectra of O-BDD, H-BDD, and PF-BDD used for peak quantification, (14) comparison of Na(1s) XPS spectra for H-BDD after electrolysis and O-BDD, (15) representative water droplet contact angle images, (16) representative current vs time curves over multiple electrolyses for each functionalized BDD electrode, (17) HTPA fluorescence calibration and normalization procedures, and (18) derivations of quantitative surface coverage equations (PDF)

■ AUTHOR INFORMATION

Corresponding Author

*E-mail: rjhamers@wisc.edu.

ORCID

Joel A. Pedersen: 0000-0002-3918-1860

Robert J. Hamers: 0000-0003-3821-9625

Author Contributions

All authors have given approval to the final version of the manuscript.

Notes

The authors declare no competing financial interest.

■ ACKNOWLEDGMENTS

This work was supported by the Wisconsin Alumni Research Foundation UW2020 initiative. The authors gratefully acknowledge use of facilities and partially supported by NSF through the University of Wisconsin Materials Research Science and Engineering Center (DMR-1720415).

■ REFERENCES

(1) Anson, C. W.; Stahl, S. S. Cooperative Electrocatalytic O_2 Reduction Involving Co(Salophen) with P-Hydroquinone as an Electron-Proton Transfer Mediator. *J. Am. Chem. Soc.* **2017**, *139*, 18472−18475.

(2) Kattel, S.; Liu, P.; Chen, J. G. G. Tuning Selectivity of Co_2 Hydrogenation Reactions at the Metal/Oxide Interface. *J. Am. Chem. Soc.* **2017**, *139*, 9739−9754.

(3) McCreery, R. L. Advanced Carbon Electrode Materials for Molecular Electrochemistry. *Chem. Rev.* **2008**, *108*, 2646−2687.

(4) Monroe, E. B.; Heien, M. L. Electrochemical Generation of Hydroxyl Radicals for Examining Protein Structure. *Anal. Chem.* **2013**, *85*, 6185−6189.

(5) Roylance, J. J.; Kim, T. W.; Choi, K. S. Efficient and Selective Electrochemical and Photoelectrochemical Reduction of 5-Hydroxymethylfurfural to 2,5-Bis(Hydroxymethyl)Furan Using Water as the Hydrogen Source. *ACS Catal.* **2016**, *6*, 1840−1847.

(6) Wang, Y. H.; Pegis, M. L.; Mayer, J. M.; Stahl, S. S. Molecular Cobalt Catalysts for O_2 Reduction: Low-Overpotential Production of H_2o_2 and Comparison with Iron-Based Catalysts. *J. Am. Chem. Soc.* **2017**, *139*, 16458−16461.

(7) Chaplin, B. P.; Schrader, G.; Farrell, J. Electrochemical Destruction of N-Nitrosodimethylamine in Reverse Osmosis Concentrates Using Boron-Doped Diamond Film Electrodes. *Environ Sci. Technol.* **2010**, *44*, 4264−4269.

(8) Gligorovski, S.; Strekowski, R.; Barbati, S.; Vione, D. Environmental Implications of Hydroxyl Radicals (•OH). *Chem. Rev.* **2015**, *115*, 13051−13092.

(9) Chaplin, B. P. Critical Review of Electrochemical Advanced Oxidation Processes for Water Treatment Applications. *Environ. Sci.: Processes Impacts* **2014**, *16*, 1182−1203.

(10) Sirés, I.; Brillas, E.; Oturan, M. A.; Rodrigo, M. A.; Panizza, M. Electrochemical Advanced Oxidation Processes: Today and Tomorrow. A Review. *Environ. Sci. Pollut. Res.* **2014**, *21*, 8336−8367.

(11) Moreira, F. C.; Boaventura, R. A. R.; Brillas, E.; Vilar, V. J. P. Electrochemical Advanced Oxidation Processes: A Review on Their Application to Synthetic and Real Wastewaters. *Appl. Catal., B* **2017**, *202*, 217−261.

(12) Enache, T. A.; Chiorcea-Paquim, A.-M.; Fatibello-Filho, O.; Oliveira-Brett, A. M. Hydroxyl Radicals Electrochemically Generated in Situ on a Boron-Doped Diamond Electrode. *Electrochem. Commun.* **2009**, *11*, 1342−1345.

(13) Marselli, B.; Garcia-Gomez, J.; Michaud, P.; Rodrigo, M. A.; Comninellis, C. Electrogeneration of Hydroxyl Radicals on Boron-Doped Diamond Electrodes. *J. Electrochem. Soc.* **2003**, *150*, D79−D83.

(14) Michaud, P.-A.; Panizza, M.; Ouattara, L.; Diaco, T.; Foti, G.; Comninellis, C. Electrochemical Oxidation of Water on Synthetic Boron-Doped Diamond Thin Film Anodes. *J. Appl. Electrochem.* **2003**, *33*, 151−154.

(15) Zhao, G.; Cui, X.; Liu, M.; Li, P.; Zhang, Y.; Cao, T.; Li, H.; Lei, Y.; Liu, L.; Li, D. Electrochemical Degradation of Refractory Pollutant Using a Novel Microstructured TiO_2 Nanotubes/Sb-Doped SnO_2 Electrode. *Environ. Sci. Technol.* **2009**, *43*, 1480−1486.

(16) Martínez-Huitle, C. A.; Quiroz, M. A.; Comninellis, C.; Ferro, S.; De Battisti, A. Electrochemical Incineration of Chloranilic Acid Using Ti/IrO_2, Pb/PbO_2 and Si/BDD Electrodes. *Electrochim. Acta* **2004**, *50*, 949−956.

(17) Zhao, G.; Zhang, Y.; Lei, Y.; Baoying, L. V.; Gao, J.; Zhang, Y.; Li, D. Fabrication and Electrochemical Treatment Application of a Novel Lead Dioxide Anode with Superhydrophobic Surfaces, High Oxygen Evolution Potential, and Oxidation Capability. *Environ. Sci. Technol.* **2010**, *44*, 1754−1759.

(18) Bejan, D.; Guinea, E.; Bunce, N. J. On the Nature of the Hydroxyl Radicals Produced at Boron-Doped Diamond and Ebonex Anodes. *Electrochim. Acta* **2012**, *69*, 275−281.

(19) Macpherson, J. V. A Practical Guide to Using Boron Doped Diamond in Electrochemical Research. *Phys. Chem. Chem. Phys.* **2015**, *17*, 2935−2949.

DOI: 10.1021/acs.langmuir.8b04030
Langmuir 2019, 35, 2153−2163

(20) Kapałka, A.; Fóti, G.; Comninellis, C. Determination of the Tafel Slope for Oxygen Evolution on Boron-Doped Diamond Electrodes. *Electrochem. Commun.* **2008**, *10*, 607−610.
(21) García-Osorio, D. A.; Jaimes, R.; Vazquez-Arenas, J.; Lara, R. H.; Alvarez-Ramirez, J. The Kinetic Parameters of the Oxygen Evolution Reaction (OER) Calculated on Inactive Anodes Via Eis Transfer Functions: •OH Formation. *J. Electrochem. Soc.* **2017**, *164*, E3321−E3328.
(22) Fischer, A. E.; Show, Y.; Swain, G. M. Electrochemical Performance of Diamond Thin-Film Electrodes from Different Commercial Sources. *Anal. Chem.* **2004**, *76*, 2553−2560.
(23) Einaga, Y. Diamond Electrodes for Electrochemical Analysis. *J. Appl. Electrochem.* **2010**, *40*, 1807−1816.
(24) Salazar-Gastélum, M. I.; Lin, S. W.; Pina-Luis, G. E.; Pérez-Sicairos, S.; Félix-Navarro, R. M. Electrochemical and Spectrometric Studies for the Determination of the Mechanism of Oxygen Evolution Reaction. *J. Electrochem. Soc.* **2016**, *163*, G37−G43.
(25) Siahrostami, S.; Li, G. L.; Viswanathan, V.; Norskov, J. K. One- or Two-Electron Water Oxidation, Hydroxyl Radical, or H_2o_2 Evolution. *J. Phys. Chem. Lett.* **2017**, *8*, 1157−1160.
(26) Swain, G. M.; Ramesham, R. The Electrochemical Activity of Boron-Doped Polycrystalline Diamond Thin-Film Electrodes. *Anal. Chem.* **1993**, *65*, 345−351.
(27) Granger, M. C.; Witek, M.; Xu, J. S.; Wang, J.; Hupert, M.; Hanks, A.; Koppang, M. D.; Butler, J. E.; Lucazeau, G.; Mermoux, M.; Strojek, J. W.; Swain, G. M. Standard Electrochemical Behavior of High-Quality, Boron-Doped Polycrystalline Diamond Thin-Film Electrodes. *Anal. Chem.* **2000**, *72*, 3793−3804.
(28) Petrini, D.; Larsson, K. Theoretical Study of the Thermodynamic and Kinetic Aspects of Terminated (111) Diamond Surfaces. *J. Phys. Chem. C* **2008**, *112*, 3018−3026.
(29) Eckert, F.; Diedenhofen, M.; Klamt, A. Towards a First Principles Prediction of pK_a: COSMO-Rs and the Cluster-Continuum Approach. *Mol. Phys.* **2010**, *108*, 229−241.
(30) Girard, H.; Simon, N.; Ballutaud, D.; Herlem, M.; Etcheberry, A. Effect of Anodic and Cathodic Treatments on the Charge Transfer of Boron Doped Diamond Electrodes. *Diamond Relat. Mater.* **2007**, *16*, 316−325.
(31) Wang, M.; Simon, N.; Charrier, G.; Bouttemy, M.; Etcheberry, A.; Li, M.; Boukherroub, R.; Szunerits, S. Distinction between Surface Hydroxyl and Ether Groups on Boron-Doped Diamond Electrodes Using a Chemical Approach. *Electrochem. Commun.* **2010**, *12*, 351−354.
(32) Notsu, H.; Yagi, I.; Tatsuma, T.; Tryk, D. A.; Fujishima, A. Surface Carbonyl Groups on Oxidized Diamond Electrodes. *J. Electroanal. Chem.* **2000**, *492*, 31−37.
(33) Hoffmann, R.; Kriele, A.; Obloh, H.; Hees, J.; Wolfer, M.; Smirnov, W.; Yang, N.; Nebel, C. E. Electrochemical Hydrogen Termination of Boron-Doped Diamond. *Appl. Phys. Lett.* **2010**, *97*, No. 052103.
(34) Goeting, C. H.; Marken, F.; Gutiérrez-Sosa, A.; Compton, R. G.; Foord, J. S. Electrochemically Induced Surface Modifications of Boron-Doped Diamond Electrodes: An X-Ray Photoelectron Spectroscopy Study. *Diamond Relat. Mater.* **2000**, *9*, 390−396.
(35) Kondo, T.; Ito, H.; Kusakabe, K.; Ohkawa, K.; Honda, K.; Einaga, Y.; Fujishima, A.; Kawai, T. Characterization and Electrochemical Properties of CF_4 Plasma-Treated Boron-Doped Diamond Surfaces. *Diamond Relat. Mater.* **2008**, *17*, 48−54.
(36) Mayrhofer, L.; Moras, G.; Mulakaluri, N.; Rajagopalan, S.; Stevens, P. A.; Moseler, M. Fluorine-Terminated Diamond Surfaces as Dense Dipole Lattices: The Electrostatic Origin of Polar Hydrophobicity. *J. Am. Chem. Soc.* **2016**, *138*, 4018−4028.
(37) Sine, G.; Ouattara, L.; Panizza, M.; Comninellis, C. Electrochemical Behavior of Fluorinated Boron-Doped Diamond. *Electrochem. Solid-State Lett.* **2003**, *6*, D9−D11.
(38) Salvadori, M. C.; Araújo, W. W. R.; Teixeira, F. S.; Cattani, M.; Pasquarelli, A.; Oks, E. M.; Brown, I. G. Termination of Diamond Surfaces with Hydrogen, Oxygen and Fluorine Using a Small, Simple Plasma Gun. *Diamond Relat. Mater.* **2010**, *19*, 324−328.
(39) Jawando, W.; Gayen, P.; Chaplin, B. P. The Effects of Surface Oxidation and Fluorination of Boron-Doped Diamond Anodes on Perchlorate Formation and Organic Compound Oxidation. *Electrochim. Acta* **2015**, *174*, 1067−1078.
(40) Popov, C.; Kulisch, W.; Bliznakov, S.; Ceccone, G.; Gilliland, D.; Sirghi, L.; Rossi, F. Surface Modification of Nanocrystalline Diamond/Amorphous Carbon Composite Films. *Diamond Relat. Mater.* **2008**, *17*, 1229−1234.
(41) Guan, B.; Zhi, J.; Zhang, X.; Murakami, T.; Fujishima, A. Electrochemical Route for Fluorinated Modification of Boron-Doped Diamond Surface with Perfluorooctanoic Acid. *Electrochem. Commun.* **2007**, *9*, 2817−2821.
(42) Foord, J. S.; Singh, N. K.; Jackman, R. B.; Gutierrez-Sosa, A.; Proffitt, S.; Holt, K. B. Reactions of Xenon Difluoride and Atomic Hydrogen at Chemical Vapour Deposited Diamond Surfaces. *Surf. Sci.* **2001**, *488*, 335−345.
(43) Gayen, P.; Chaplin, B. P. Fluorination of Boron-Doped Diamond Film Electrodes for Minimization of Perchlorate Formation. *Appl. Mater. Interfaces* **2017**, 27638.
(44) Harris, S. J.; Belton, D. N. Thermochemistry on a Fluorinated Diamond(111) Surface. *Appl. Phys. Lett.* **1991**, *59*, 1949−1951.
(45) Saran, M.; Summer, K. H. Assaying for Hydroxyl Radicals: Hydroxylated Terephthalate Is a Superior Fluorescence Marker Than Hydroxylated Benzoate. *Free Radical Res.* **1999**, *31*, 429−436.
(46) Page, S. E.; Arnold, W. A.; McNeill, K. Terephthalate as a Probe for Photochemically Generated Hydroxyl Radical. *J. Environ. Monit.* **2010**, *12*, 1658−1665.
(47) Matthews, R. W. The Radiation Chemistry of the Terephthalate Dosimeter. *Radiat. Res.* **1980**, *83*, 27−41.
(48) Linxiang, L.; Abe, Y.; Nagasawa, Y.; Kudo, R.; Usui, N.; Imai, K.; Mashino, T.; Mochizuki, M.; Miyata, N. An Hplc Assay of Hydroxyl Radicals by the Hydroxylation Reaction of Terephthalic Acid. *Biomed. Chromatogr.* **2004**, *18*, 470−474.
(49) Strother, T.; Knickerbocker, T.; Russell, J. N.; Butler, J. E.; Smith, L. M.; Hamers, R. J. Photochemical Functionalization of Diamond Films. *Langmuir* **2002**, *18*, 968−971.
(50) Nichols, B. M.; Butler, J. E.; Russell, J. N.; Hamers, R. J. Photochemical Functionalization of Hydrogen-Terminated Diamond Surfaces: A Structural and Mechanistic Study. *J. Phys. Chem. B* **2005**, *109*, 20938−20947.
(51) Colavita, P. E.; Streifer, J. A.; Sun, B.; Wang, X.; Warf, P.; Hamers, R. J. Enhancement of Photochemical Grafting of Terminal Alkenes at Surfaces Via Molecular Mediators: The Role of Surface-Bound Electron Acceptors. *J. Phys. Chem. C* **2008**, *112*, 5102−5112.
(52) Shirley, D. A. High-Resolution X-Ray Photoemission Spectrum of the Valence Bands of Gold. *Phys. Rev. B* **1972**, *5*, 4709−4714.
(53) Jing, Y.; Chaplin, B. P. A Mechanistic Study of the Validity of Using Hydroxyl Radical Probes to Characterize Electrochemical Advanced Oxidation Processes. *Environ. Sci. Technol.* **2017**, *51*, 2355−2365.
(54) Starkweather, H. W. Melting and crystalline transitions in normal perfluoroalkanes and poly(tetrafluoroethylene). *Macromolecules* **1986**, *19*, 1131−1134.
(55) Wang, X.; Colavita, P. E.; Streifer, J. A.; Butler, J. E.; Hamers, R. J. Photochemical Grafting of Alkenes onto Carbon Surfaces: Identifying the Roles of Electrons and Holes. *J. Phys. Chem. C* **2010**, *114*, 4067−4074.
(56) Wang, X.; Landis, E. C.; Franking, R.; Hamers, R. J. Surface Chemistry for Stable and Smart Molecular and Biomolecular Interfaces Via Photochemical Grafting of Alkenes. *Acc. Chem. Res.* **2010**, *43*, 1205−1215.
(57) Ruther, R. E.; Cui, Q.; Hamers, R. J. Conformational Disorder Enhances Electron Transfer through Alkyl Monolayers: Ferrocene on Conductive Diamond. *J. Am. Chem. Soc.* **2013**, *135*, 5751−5761.
(58) Barazesh, J. M.; Prasse, C.; Sedlak, D. L. Electrochemical Transformation of Trace Organic Contaminants in the Presence of Halide and Carbonate Ions. *Environ. Sci. Technol.* **2016**, *50*, 10143−10152.

DOI: 10.1021/acs.langmuir.8b04030
Langmuir 2019, 35, 2153−2163

(59) Martin, H. B.; Argiotia, A.; Angus, J. C.; Landau, U. Voltammetry Studies of Single-Crystal and Polycrystalline Diamond Electrodes. *J. Electrochem. Soc.* **1999**, *146*, 2959.
(60) Schröder, H. F.; Meesters, R. J. W. Stability of Fluorinated Surfactants in Advanced Oxidation Processes — a Follow up of Degradation Products Using Flow Injection – Mass Spectrometry, Liquid Chromatography – Mass Spectrometry and Liquid Chromatography – Multiple Stage Mass Spectrometry. *J. Chromatogr. A* **2005**, *1082*, 110–119.
(61) Zhang, L. H.; Hamers, R. J. Photocatalytic Reduction of CO_2 to CO by Diamond Nanoparticles. *Diamond Relat. Mater.* **2017**, *78*, 24–30.
(62) Ohashi, T.; Zhang, J.; Takasu, Y.; Sugimoto, W. Steam Activation of Boron Doped Diamond Electrodes. *Electrochim. Acta* **2011**, *56*, 5599–5604.
(63) Liu, F. B.; Wang, J. D.; Liu, B.; Li, X. M.; Chen, D. R. Effect of Electronic Structures on Electrochemical Behaviors of Surface-Terminated Boron-Doped Diamond Film Electrodes. *Diamond Relat. Mater.* **2007**, *16*, 454–460.
(64) Björkman, H.; Ericson, C.; Hjertén, S.; Hjort, K. Diamond Microchips for Fast Chromatography of Proteins. *Sens. Actuators, B* **2001**, *79*, 71–77.
(65) Yagi, I.; Notsu, H.; Kondo, T.; Tryk, D. A.; Fujishima, A. Electrochemical Selectivity for Redox Systems at Oxygen-Terminated Diamond Electrodes. *J. Electroanal. Chem.* **1999**, *473*, 173–178.
(66) Hutton, L. A.; Iacobini, J. G.; Bitziou, E.; Channon, R. B.; Newton, M. E.; Macpherson, J. V. Examination of the Factors Affecting the Electrochemical Performance of Oxygen-Terminated Polycrystalline Boron-Doped Diamond Electrodes. *Anal. Chem.* **2013**, *85*, 7230–7240.
(67) Lew, H.; Heiber, I. Spectrum of H_2O^+. *J. Chem. Phys.* **1973**, *58*, 1246–1247.
(68) Hochanadel, C. J. Effects of Cobalt γ-Radiation on Water and Aqueous Solutions. *J. Phys. Chem.* **1952**, *56*, 587–594.
(69) Hart, E. J. The Radical Pair Yield of Ionizing Radiation in Aqueous Solutions of Formic Acid. *J. Phys. Chem.* **1952**, *56*, 594–599.
(70) Joshi, A. A.; Locke, B. R.; Arce, P.; Finney, W. C. Formation of Hydroxyl Radicals, Hydrogen Peroxide and Aqueous Electrons by Pulsed Streamer Corona Discharge in Aqueous Solution. *J. Hazard. Mater.* **1995**, *41*, 3–30.
(71) Chaplin, B. P.; Hubler, D. K.; Farrell, J. Understanding Anodic Wear at Boron Doped Diamond Film Electrodes. *Electrochim. Acta* **2013**, *89*, 122–131.

DOI: 10.1021/acs.langmuir.8b04030
Langmuir 2019, 35, 2153–2163